Research Article | Vol. 31, No. 11 / 22 May 2023 / Optics Express 17165
Optics EXPRESS

Coherent OTDR with large dynamic range based on double-sideband linear frequency modulation pulse

YUYAO WANG,[1] HUA ZHENG,[1,*] HUAN WU,[1] DONGMEI HUANG,[2] CHANGYUAN YU,[1] AND CHAO LU[1]

[1] *Photonics Research Institute, Department of Electronic and Information Engineering, The Hong Kong Polytechnic University, Hong Kong, China*
[2] *Photonics Research Institute, Department of Electrical Engineering, The Hong Kong Polytechnic University, Hong Kong, China*
[*] *hua.zheng@polyu.edu.hk*

Abstract: Rayleigh scattering-based distributed optical fiber sensors with long sensing distance and large dynamic range are highly desired for application scenarios such as vehicle tracking, structure health monitoring, and geological survey. To enlarge the dynamic range, we propose a coherent optical time domain reflectometry (COTDR) based on double-sideband linear frequency modulation (LFM) pulse. By utilizing I/Q demodulation, both the positive and negative frequency band of the Rayleigh backscattering (RBS) signal can be properly demodulated. Consequently, the dynamic range is doubled without increasing the bandwidth of signal generator, photodetector (PD), and oscilloscope. In the experiment, the chirped pulse with 10 μs pulse width and 498 MHz frequency sweeping range is launched into the sensing fiber. Single-shot strain measurement is achieved over 5 km single-mode fiber with a spatial resolution of 2.5 m and a strain sensitivity of 7.5 $p\varepsilon/\sqrt{Hz}$. A vibration signal with 3.09 $\mu\varepsilon$ peak-to-peak amplitude (corresponding to 461 MHz frequency shift) is successfully measured with the double-sideband spectrum, which cannot be properly recovered with the single-sideband spectrum.

1. Introduction

Coherent optical time domain reflectometry has been widely studied owing to its merits of high sensitivity, long-distance monitoring, and accurate localization [1–3]. The dependence of fiber refractive index on temperature and strain enables COTDR to track these variables precisely, which makes it a reliable tool in a variety of application scenarios [4]. Based on different detection methods, COTDR can be roughly divided into direct detection OTDR [5] and coherent detection OTDR [6–8], which have demonstrated their ultrahigh precision temperature/strain and vibration measurement ability, respectively.

In coherent detection OTDR, the strain information is usually obtained from the phase difference of Rayleigh backscattering (RBS) trace at different positions, which can be achieved by using heterodyne [9,10] or homodyne [11,12] method. In the demodulation process, phase unwrapping is used to obtain the continuous strain induced by the vibration, and the phase difference between adjacent points needs to be less than π *rad*. Therefore, the amplitude of the vibration, especially for high frequency signal, is restricted, which limits the application of the system in large dynamic strain measurements [13]. In direct detection OTDR, the strain and temperature are demodulated from the frequency spectrum of RBS, and the dynamic range is merely limited by the frequency span of probe pulses. In this scheme, a pulse sequence with different frequencies is launched into the sensing fiber to obtain the frequency spectrum. The temperature or strain variation can be derived from the cross-correlation between a reference spectrum and a live spectrum measured at two different time stamps. With this technique,

#485616 https://doi.org/10.1364/OE.485616
Journal © 2023 Received 13 Jan 2023; revised 21 Apr 2023; accepted 21 Apr 2023; published 8 May 2023

Optics EXPRESS

distributed temperature measurement was achieved on an 8-km-long fiber with a temperature resolution of 0.01 ℃ and a spatial resolution of 1 m [6]. Alternatively, chirped pulse can be employed as probe to convert the frequency shift in frequency domain to a time shift along the RBS trace. Temperature/strain resolutions of $1mK/4n\varepsilon$ was demonstrated over 1-km fiber with single-shot measurement [14]. Nevertheless, both in frequency scanning COTDR and chirped pulse COTDR, the spatial resolution is determined by the pulse width, resulting in a tradeoff between the spatial resolution and the sensing distance. More recently, a chirped-pulse COTDR based on coherent detection was proposed [15,16], in which the RBS signal can be extracted with the usage of non-matched filter [17] or sub-chirped-pulse extraction algorithm [18,19]. The spatial resolution of such system is determined by the bandwidth of matched filter rather than the pulse width. As a result, distributed sensing with high spatial resolution and long sensing distance can be realized at the same time. Distributed strain measurements were demonstrated on a 75 km fiber with a strain sensitivity better than 100 $p\varepsilon/\sqrt{Hz}$ and a spatial resolution of 2 m [18].

To further enhance the dynamic range of COTDR, in this paper, we proposed the COTDR based on double-sideband chirped pulse. With I/Q demodulation, both the positive and negative frequency band of RBS can be utilized, thus, the frequency spectrum range is doubled without increasing the bandwidth of hardware. Large vibration with an amplitude of 3.09 $\mu\varepsilon$ (corresponding to 461 MHz frequency shift) is successfully measured. Single-shot strain measurement is achieved over 5 km single mode fiber with a spatial resolution of 2.5 m and a strain sensitivity of 7.5 $p\varepsilon/\sqrt{Hz}$. Since the strain is demodulated by estimating the frequency shift of RBS spectrum, the proposed scheme is immune to fading caused by destructive interference or polarization misalignment. The rest of the paper is organized as follows: Section 2 illustrates the measurement principle; Section 3 describes the experimental setup and the system parameters; then the experimental results are demonstrated in Section 4; finally, a brief conclusion is given in Section 5.

2. Principle

2.1. Principle of COTDR based on double frequency sidebands

In a Mach–Zehnder electro-optic intensity modulator (EOM), the input optical signal is equally split into two arms and then recombined. Supposing that the phase delays of the two MZI arms are φ_1 and φ_2, the input optical fields is E_i, the output optical field E_o can be written as:

$$E_o = \frac{1}{2}(e^{j\varphi_1} + e^{j\varphi_2})E_i = \cos(\frac{\varphi_1 - \varphi_2}{2})e^{j\frac{\varphi_1+\varphi_2}{2}}E_i \tag{1}$$

The phase shifts of the two arms are given by:

$$\varphi_1 = \varphi_0 + \frac{\pi V_{AC}(t)}{2V_\pi} \tag{2}$$

$$\varphi_2 = \frac{\pi[V_{bias} - V_{AC}(t)]}{2V_\pi} \tag{3}$$

where φ_0 is the phase difference between the two arms. V_{bias} represents the bias voltage and the modulation voltage can be written as $V_{AC}(t) = V_{AC}\cos(\omega_{AC}t)$, respectively. V_π is the half-wave

Optics EXPRESS

voltage of modulator. Equation (1) can be expanded as follows according to *Bessel* function:

$$\begin{aligned} E_o(t) = E_i e^{j[\varphi_0 + \frac{\pi V_{bias}}{2V_\pi}]} \Bigg\{ & \cos(\varphi_0 - \frac{\pi V_{bias}}{2V_\pi}) J_0(\frac{\pi V_{AC}}{V_\pi}) \\ & + 2\cos(\varphi_0 - \frac{\pi V_{bias}}{2V_\pi}) \sum_{n=1}^{\infty} (-1)^n J_{2n}(\frac{\pi V_{AC}}{2V_\pi}) \cos(2n\omega_{AC}t) \\ & -2\sin(\varphi_0 - \frac{\pi V_{bias}}{2V_\pi}) \sum_{n=0}^{\infty} (-1)^n J_{2n+1}(\frac{\pi V_{AC}}{2V_\pi}) \cos[(2n+1)\omega_{AC}t] \Bigg\} \end{aligned} \tag{4}$$

where $J_n()$ is the n-order *Bessel* function. When φ_0-$(\pi V_{bias})/2V_\pi$=$\pi/2$ and $\pi V_{AC}/2V_\pi \ll 1$ are satisfied, the modulator is working at the null point, and the optical carrier and the higher order sidebands are suppressed. Only the positive and negative first-order sidebands need to be considered. In this case, Eq. (4) can be simplified as:

$$\begin{aligned} E_o(t) &= E_i e^{j[\varphi_0 + \frac{\pi V_{bias}}{2V_\pi}]} \left[-2J_1(\frac{\pi V_{AC}}{2V_\pi}) \cos(\omega_{AC}t) \right] \\ &= E_i e^{j[\varphi_0 + \frac{\pi V_{bias}}{2V_\pi}]} \cdot \left\{ -J_1(\frac{\pi V_{AC}}{2V_\pi}) \cdot [\exp(j\omega_{AC}t) + \exp(-j\omega_{AC}t)] \right\} \end{aligned} \tag{5}$$

In pulse compression COTDR, the light is modulated into LFM pulses by the modulator. The phase variation caused by the modulator can be written as:

$$\theta(t) = (2\pi f_0 t + \pi\kappa t^2) \cdot rect\left(\frac{t}{T}\right) \tag{6}$$

And the output light field of modulator $E_o(t)$ can be written as

$$E_o(t) = -J_1(\frac{\pi\gamma}{2}) E_i e^{j[\varphi_0 + \frac{\pi V_{bias}}{2V_\pi}]} \cdot \{\exp[j(2\pi f_c t + \theta(t))] + \exp[j(2\pi f_c t - \theta(t))]\} rect\left(\frac{t}{T}\right) \tag{7}$$

where γ=V_{AC}/V_π is the modulation depth, $f_c, f_{0,}$ and κ represent the optical carrier frequency, initial sweeping frequency, and the slope of LFM pulse respectively, T denotes the pulse width. The LFM pulse is launched into the fiber under test (FUT), and the RBS signal is mixed with the local oscillator (LO) to obtain the beat signal. The RBS signal and the LO can be expressed as:

$$E_{RBS}(t) = \sum_{i=1}^{N} r_i \exp\left(-\alpha \frac{c\tau_i}{n}\right) E_0(t - \tau_i) \tag{8}$$

$$E_L(t) = E_{LO} \exp(j2\pi f_c t) \tag{9}$$

Using an optical hybrid coupler, the complex field of the beat signal can be recovered with the in-phase (I) and quadrature (Q) components:

$$\begin{aligned} E_s(t) &= I(t) + jQ(t) \\ &= \sum_{i=1}^{N} a_i \cdot \{\exp[j(-2\pi f_c \tau_i + \theta(t - \tau_i))] + \exp[j(-2\pi f_c \tau_i - \theta(t - \tau_i))]\} rect\left(\frac{t - \tau_i}{T}\right) \end{aligned} \tag{10}$$

In the above equations, a_i, r_i and τ_i represent the amplitude and time delay of light reflected by the i-th reflector in FUT, α is the attenuation coefficient of fiber. As shown in Eq. (10) and Fig. 1, the detected complex signal contains two frequency sidebands with different information. The RBS signals with different frequencies can be derived using matched filters with different

Optics EXPRESS

frequency sweeping ranges. Hypothesizing sub-chirped pulse sequence with initial frequency f_k and duration T_1 is used to perform matched filtering on positive and negative band respectively:

$$\begin{aligned} h_+(t) &= \exp\{j(2\pi f_k t + \pi\kappa t^2)\} rect(t/T_1), \ and \\ h_-(t) &= \exp\{-j(2\pi f_k t + \pi\kappa t^2)\} rect(t/T_1) \end{aligned} \tag{11}$$

The compressed signal of *k-th* matched filter can be deduced according to Eq. (10) and (11):

$$\begin{aligned} s(t) &= E_s(t) * h_{+/-}(t) \\ &= -J_1(\frac{\pi\gamma}{2}) E_{Lo} E_i e^{j[\varphi_0 + \frac{\pi V_{bias}}{2V_\pi}]} h_{FUT} * \left[\frac{\sin[\pi\kappa(T_1 - |t|)t]}{\pi\kappa t} \cdot \exp\left(\pm j2\pi(f_k + \frac{\kappa T_1}{2})t \right) \right] \end{aligned} \tag{12}$$

where $h_{FUT} = \sum_{i=1}^{N} r_i \exp(-\alpha \frac{c\tau_i}{n}) \cdot \exp\{-j2\pi f_c \tau_i\} \cdot \delta(t - \tau_i)$ is the impulse response of FUT. As can be seen from the above deduction that the compressed signal is the convolution of h_{FUT} and a *sinc* function with different frequencies. Therefore, an RBS spectrum as the function of time and frequency $s(t,f)$ can be constructed using matched filters with different center frequencies. The spatial resolution *SR* is defined as the full width at half-maximum (FWHM) of the main lobe of the *sinc* function:

$$SR = \frac{c}{2n\kappa T_1} \tag{13}$$

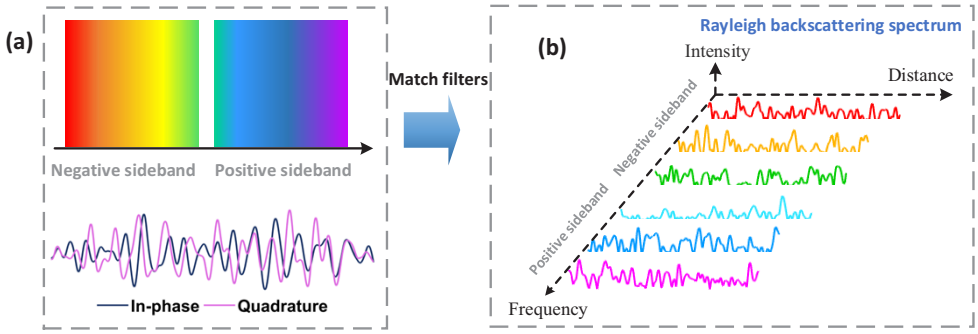

Fig. 1. Principle of COTDR based on double frequency sidebands: (a) Detected RBS traces and the corresponding frequency spectrum; (b) Rayleigh backscattering spectrum.

2.2. *Dynamic strain demodulation principle*

When a strain is applied to the fiber, the phase difference ($\Delta\varphi$) of RBS between position z_i and z_j will change accordingly, which can be expressed as [20]

$$\begin{aligned} \Delta\varphi_{ij} &= \frac{4\pi f_c}{c}(n \cdot \Delta z_{ij} + \Delta n \cdot z_{ij}) \\ &= \frac{4\pi f_c}{c}(n + C_\varepsilon) \cdot z_{ij} \Delta\varepsilon \end{aligned} \tag{14}$$

where f_c, c, n, and z_{ij} are the optical frequency, optical velocity, refractive index of fiber, and the distance between i-th and j-th scattering points in fiber, respectively. Δz_{ij} and Δn represent the variation of z_{ij} and n caused by strain, respectively. C_ε is the refractive index strain parameter, and

Optics EXPRESS

$\Delta\varepsilon$ represents the magnitude of strain. The phase change can be compensated by the frequency shift (f_{shift}) of pulses:

$$\Delta\varphi_{ij} = \frac{4\pi n z_{ij}}{c} f_{shift} \tag{15}$$

As reported in [6], the frequency shift to compensate the phase change is given by:

$$\frac{f_{shift}}{f_c} = -0.78 \times \Delta\varepsilon \tag{16}$$

To estimate the frequency shift of RBS with a frequency spectrum range F, a least mean square (LMS) algorithm is applied between the reference RBS spectrum S_{ref} and the measurement RBS spectrum S_{mea}. The mean square error with a frequency shift of δf is given by [21]:

$$R_{ref,mea}(t,\delta f) = \frac{1}{F-|\delta f|} \cdot \sum_{f=-(F-|\delta f|)}^{F-|\delta f|} [s_{ref}(t,f+\delta f) - s_{mea}(t,f)]^2 \tag{17}$$

Then the frequency shift can be estimated as:

$$f_{shift}(t) = \arg\min_{\delta f}[R_{ref,mea}(t,\delta f)] \tag{18}$$

3. Experimental setup

The experimental setup is shown in Fig. 2. The continuous light emitted by a narrow linewidth laser source operating at 1550 nm was split by a 90:10 coupler. Then the light in upper branch was modulated into a chirped pulse by an EOM driven by an arbitrary waveform generator (AWG). The frequency sweeping range of the chirp pulse ranged from 2 MHz to 500 MHz, the pulse width and pulse period were 10 μs and 150 μs respectively. An erbium-doped fiber amplifier (EDFA) and a bandpass filter were used to amplify the power of the chirp pulse and remove the amplified spontaneous emission (ASE) noise. Later, the amplified pulse was injected into a 5-km sensing fiber. And the Rayleigh backscattering light was amplified and filtered by another group of EDFA and bandpass filter. In our experiment, the length of fiber of PZT was 10 m and it was put at the far end of the 5 km sensing fiber. In lower branch, a polarization controller (PC) was used to adjust the polarization state of the LO. Finally, the LO in lower branch and the backscattering signal were mixed in an optical hybrid. Two photodetectors with 500 MHz bandwidths were used to receive the in-phase (I) and quadrature (Q) components and the detected signals were sent to the oscilloscope to be collected at the sampling rate of 2 GSa/s.

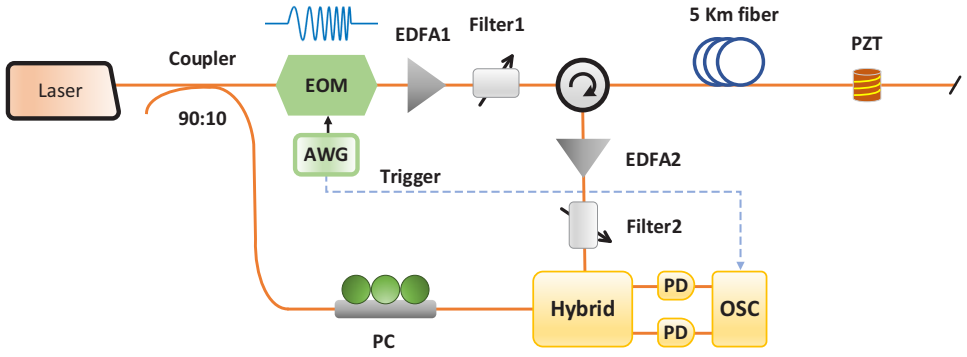

Fig. 2. Experimental setup. EOM: electro-optic modulator; AWG: arbitrary waveform generator; EDFA: erbium-doped fiber amplifier; PC: polarization controller; PZT: piezoelectric ceramics; PD: photodetector; OSC: oscilloscope.

Optics EXPRESS

4. Experimental results

Figure 3 shows the calculated Rayleigh backscattering spectrum after match filtering. In our demodulation process, the bandwidth of matched filter is set to be 40 MHz and the frequency interval between adjacent filters is 4 MHz, which results in 114 traces available for each sideband. It should be noted that 44 MHz frequency spectrum around carrier frequency is not available (interpolate to 0 in Fig. 3), since the initial sweeping frequency of chirped pulse is 2 MHz. The interpolated part will not affect the frequency shift estimation, because it is abandoned during the LMS process. To improve the accuracy, the frequency interval is interpolated to be 0.04 MHz by using cubic polynomial interpolation with a factor of 100.

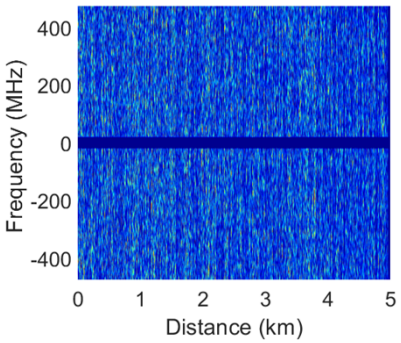

Fig. 3. Rayleigh backscattering spectrum after match filtering.

Figure 4 shows the calculated frequency shift versus time and distance near the end of FUT. The applied voltage and frequency are 1 V and 100 Hz, respectively. A disturbed area can be clearly identified from 4960 m to 4970 m in Fig. 4(a). Figure 4(b) is the time trace of vibration at 4965 m, we can see that the *sine* waveform is well recovered with the LMS algorithm

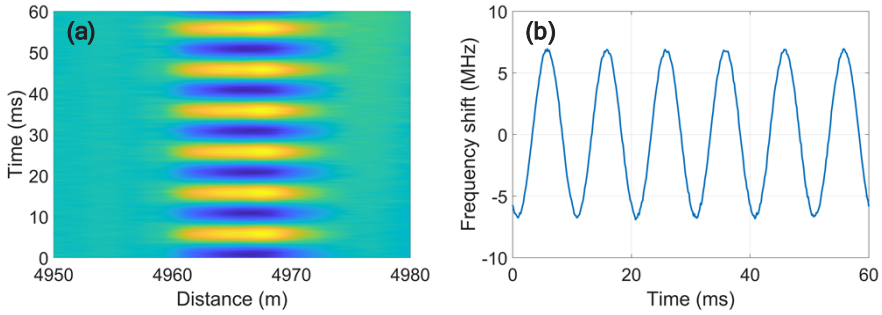

Fig. 4. (a) Frequency shift caused by strain at the end of FUT. (b) Vibration at 4965 m.

Then we measured the vibration signals with different amplitudes and different frequencies. The measurement results are displayed in Fig. 5. The vibration voltages applied to the PZT changed from 0.2 V to 10 V in Fig. 5(a), and the frequency was kept at 100 Hz. The frequency shift coefficient is 13.63 MHz/V, and the coefficient of determination is 0.9999, indicating a good linear relationship between the frequency shift and the amplitude of the vibration. Figure 5(b) depicts the measurement results of vibrations with an amplitude of 5 V and frequencies ranging from 200 Hz to 800 Hz, which are in good agreement with the applied signals.

To investigate the dynamic range of our method, we used a piezo controller to amplify the vibration signal applied to the PZT. The pulse width and pulse period are 10 μs and 80 μs

Optics EXPRESS

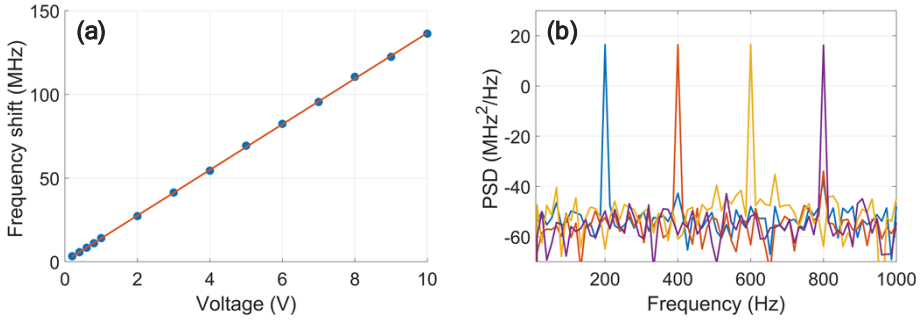

Fig. 5. (a) Frequency shifts of RBS at different voltage; (b) measured frequency spectra of different frequency vibrations.

respectively in this case. Figures 6(a), (b) and (c) show the measurement results of vibrations with frequencies of 200 Hz, 500 Hz, 1 KHz and amplitudes of 31 V, 34 V, and 32 V, respectively. The frequency shifts reach 424 MHz, 461 MHz, and 434 MHz, respectively. We can see that the results demodulated from the single-sideband frequency spectra are distorted, while the waveforms can be perfectly retrieved from the double-sideband spectra, proving the effectiveness of the proposed method. In the demodulation process, a fixed reference RBS spectrum is used, and the maximum frequency shift between the measured spectrum and reference spectrum is 267 MHz (in Fig. 6(b)). The strain range can be extended by calculating the frequency shifts between every two consecutive RBS spectra and then integrating the frequency shifts along the time axis.

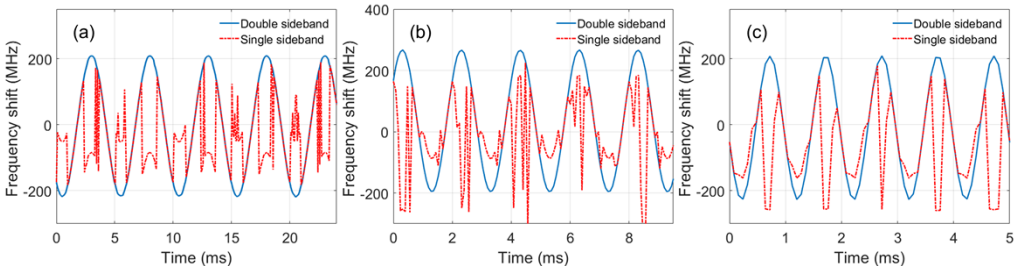

Fig. 6. Measurement results of large amplitude vibrations with frequencies of (a) 200 Hz; (b) 500 Hz; (c) 1 KHz. (Blue: double sideband; Red: single sideband).

Figure (7) shows the frequency spectra of the same data in Fig. 6(a) at 4.08 *ms* and 4.96 *ms*, with a frequency shift of 222 MHz in between. Figure 7(a) shows the double sideband frequency spectra, where the 44 MHz missing frequency points are drawn with dashed lines. Figure 7(b) shows the double sideband frequency spectra after 222 MHz frequency shift. The gray and red shaded areas are used to estimate the mean square error with LMS algorithm. The unshaded areas with dashed lines are invalid areas which are discarded in the calculation process to avoid frequency shift estimation error. Figure 7(c) shows the positive sideband in Fig. 7(a), and Fig. 7(d) shows the frequency shifted positive sideband spectra. The red shaded area which is used to estimate frequency shift is corresponding to the red shaded area in Fig. 7(b). It can be seen from Fig. 7(d) that the frequency shift reaches almost half of the spectrum range, in which circumstance the frequency shift is easily estimated incorrectly. But in Fig. 7(b), the valid area is larger, and the frequency shift can be estimated more accurately.

In the pulse compression scheme, the spatial resolution of the system is no longer restricted by the pulse width but determined by the bandwidth of matched filters. Therefore, long pulses can

Optics EXPRESS

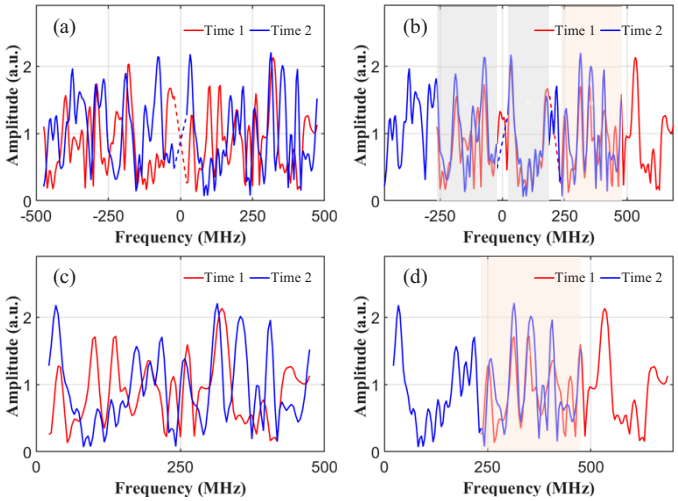

Fig. 7. (a) Double-sideband frequency spectra two different times; (b) frequency shifted double sideband spectra; (c) positive sideband frequency spectra; (d) frequency shifted positive sideband spectra.

be used to improve the SNR of the signal. According to Eq. (13), a matched filter with 40 MHz bandwidth will lead to a spatial resolution of 2.5 m, as indicated in Fig. 8(a). To evaluate the noise level of the system, the power spectral density (PSD) along the fiber distance is calculated. As shown in Fig. 8(b), the maximum averaged PSD between 500 Hz and 3 kHz is −59 dB, corresponding to a strain sensitivity of 7.5 $p\varepsilon/\sqrt{Hz}$. Compared with the phase demodulation scheme, interference and polarization fading free measurement is achieved over the entire FUT.

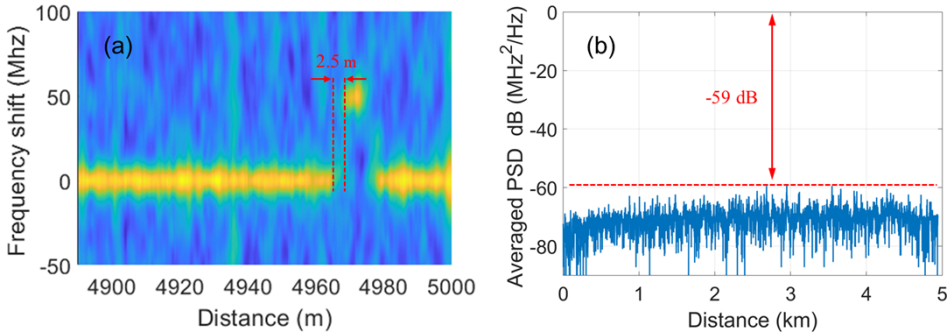

Fig. 8. (a) Spatial resolution of the system; (b) averaged power spectral density between 500 Hz and 3000 Hz along the fiber.

To further demonstrate the performance of double-sideband COTDR, complex waveforms are applied to the PZT. The pulse width and pulse period are set to be 10 μs and 150 μs respectively. Figure 9 shows the measurement results of chirped waveform (a-c) and triangle waveform (d-f). The chirped waveform swept from 100 Hz to 1000 Hz with a duration of 20 ms and an amplitude of 2 V. From the time-frequency map in Fig. 9(c), we can see that the chirped waveform is well recovered. The frequency and amplitude of the triangle wave are 300 Hz and 2 V respectively. The measurement results are in good agreement with the actual situation, demonstrating the reliability of the system.

Optics EXPRESS

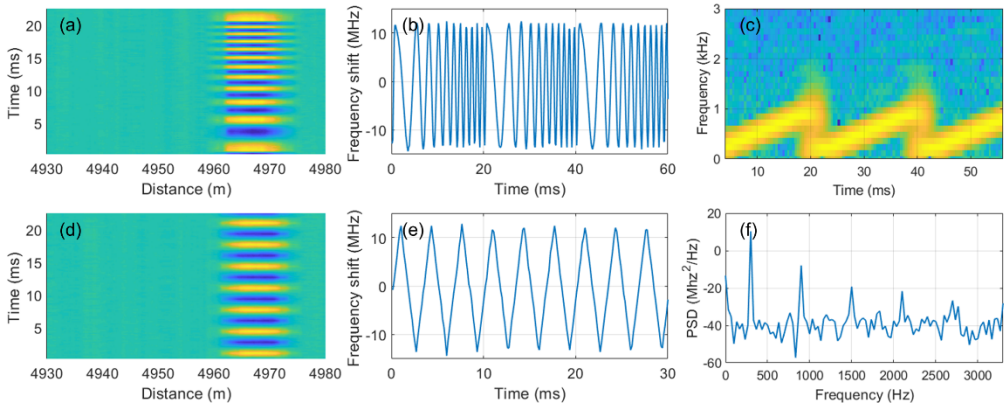

Fig. 9. (a)-(c): Frequency shift, time-domain waveform, and time-frequency map of chirped wave; (d)-(f): Frequency shift, time-domain waveform, and frequency spectra of triangle wave.

5. Conclusion

In this paper, we proposed a COTDR based on double-sideband linear frequency modulation (LFM) pulse. By making full use of both positive and negative frequency bands of RBS spectrum, the dynamic range can be doubled without increasing the bandwidth of electronic equipment in system. Interference and polarization fading free distributed strain measurement is achieved over 5 km single-mode fiber by employing a double sideband LFM pulse with 10 μs pulse width and 498 MHz frequency sweeping range. The spatial resolution of the system is 2.5 m and the strain sensitivity is higher than 7.5 $p\varepsilon/\sqrt{Hz}$. The proposed scheme is expected to be used in large vibration signal measurement.

Funding. Research Grant Council of the Hong Kong SAR Government (PolyU, 15209919); Technology and Innovation Commission of Shenzhen Municipality (JCYJ20210324133406018); Postdoc Matching Fund Scheme of the Hong Kong Polytechnic University (1-W23E).

Disclosures. The authors declare no conflicts of interest

Data availability. Data underlying the results presented in this paper are not publicly available at this time but may be obtained from the authors upon reasonable request.

References

1. F. Peng, H. Wu, X.-H. Jia, Y.-J. Rao, Z.-N. Wang, and Z.-P. Peng, "Ultra-long high-sensitivity Φ-OTDR for high spatial resolution intrusion detection of pipelines," Opt. Express **22**(11), 13804–13810 (2014).
2. T. Zhu, X. Xiao, Q. He, and D. Diao, "Enhancement of SNR and Spatial Resolution in j-OTDR System by Using Two-Dimensional Edge Detection Method," J. Lightwave Technol. **31**(17), 2851–2856 (2013).
3. Y. Wu, Z. Wang, J. Xiong, J. Jiang, and Y. Rao, "Bipolar-Coding Φ-OTDR with Interference Fading Elimination and Frequency Drift Compensation," J. Lightwave Technol. **38**(21), 6121–6128 (2020).
4. Y. Lu, T. Zhu, L. Chen, and X. Bao, "Distributed vibration sensor based on coherent detection of phase-OTDR," J. Lightwave Technol. **28**(22), 3243–3249 (2010).
5. L. Zhang, Z. Yang, N. Gorbatov, R. Davidi, M. Galal, L. Thévenaz, and M. Tur, "Distributed and dynamic strain sensing with high spatial resolution and large measurable strain range," Opt. Lett. **45**(18), 5020–5023 (2020).
6. Y. Koyamada, M. Imahama, K. Kubota, and K. Hogari, "Fiber-optic distributed strain and temperature sensing with very high measurand resolution over long range using coherent OTDR," J. Lightwave Technol. **27**(9), 1142–1146 (2009).
7. G. Yang, X. Fan, S. Wang, B. Wang, Q. Liu, and Z. He, "Long-range distributed vibration sensing based on phase extraction from phase-sensitive OTDR," IEEE Photonics J. **8**(3), 1–12 (2016).
8. D. Chen, Q. Liu, and Z. He, "Phase-detection distributed fiber-optic vibration sensor without fading-noise based on time-gated digital OFDR," Opt. Express **25**(7), 8315–8325 (2017).
9. Q. Yan, M. Tian, X. Li, Q. Yang, and Y. Xu, "Coherent φ-OTDR based on polarization-diversity integrated coherent receiver and heterodyne detection," in *25th Optical Fiber Sensors Conference* (IEEE, 2017), pp. 1–4.

Optics EXPRESS

10. X. He, S. Xie, F. Liu, S. Cao, L. Gu, X. Zheng, and M. Zhang, "Multi-event waveform-retrieved distributed optical fiber acoustic sensor using dual-pulse heterodyne phase-sensitive OTDR," Opt. Lett. **42**(3), 442–445 (2017).
11. Z. Wang, L. Zhang, S. Wang, N. Xue, F. Peng, M. Fan, W. Sun, X. Qian, J. Rao, and Y. Rao, "Coherent Φ-OTDR based on I/Q demodulation and homodyne detection," Opt. Express **24**(2), 853–858 (2016).
12. Y. Yan, H. Zheng, Z. Zhao, C. Guo, X. Wu, J. Hu, A. P. T. Lau, and C. Lu, "Distributed optical fiber sensing assisted by optical communication techniques," J. Lightwave Technol. **39**(12), 3654–3670 (2021).
13. F. Cunzheng, L. Hao, H. Tao, Z. Shixiong, Y. Baoqiang, Y. Zhijun, and S. Qizhen, "Large dynamic range optical fiber distributed acoustic sensing (DAS) with differential-unwrapping-integral algorithm," J. Lightwave Technol. **39**(22), 7274–7280 (2021).
14. J. Pastor-Graells, H. F. Martins, A. Garcia-Ruiz, S. Martin-Lopez, and M. Gonzalez-Herraez, "Single-shot distributed temperature and strain tracking using direct detection phase-sensitive OTDR with chirped pulses," Opt. Express **24**(12), 13121–13133 (2016).
15. D. Chen, Q. Liu, and Z. He, "High-fidelity distributed fiber-optic acoustic sensor with fading noise suppressed and sub-meter spatial resolution," Opt. Express **26**(13), 16138–16146 (2018).
16. K. Kishida, A. Guzik, K. Nishiguchi, C.-H. Li, D. Azuma, Q. Liu, and Z. He, "Development of real-time time gated digital (TGD) OFDR method and its performance verification," Sensors **21**(14), 4865 (2021).
17. D. Chen, Q. Liu, Y. Wang, H. Li, and Z. He, "Fiber-optic distributed acoustic sensor based on a chirped pulse and a non-matched filter," Opt. Express **27**(20), 29415–29424 (2019).
18. J. Xiong, Z. Wang, Y. Wu, and Y. Rao, "Single-shot COTDR using sub-chirped-pulse extraction algorithm for distributed strain sensing," J. Lightwave Technol. **38**(7), 2028–2036 (2020).
19. Y. Wang, Q. Liu, D. Chen, H. Li, and Z. He, "Distributed fiber-optic dynamic-strain sensor with sub-meter spatial resolution and single-shot measurement," IEEE Photonics J. **11**(6), 1–8 (2019).
20. Y. Dong, X. Chen, E. Liu, C. Fu, H. Zhang, and Z. Lu, "Quantitative measurement of dynamic nanostrain based on a phase-sensitive optical time domain reflectometer," Appl. Opt. **55**(28), 7810–7815 (2016).
21. S. Liehr, S. Münzenberger, and K. Krebber, "Wavelength-scanning coherent OTDR for dynamic high strain resolution sensing," Opt. Express **26**(8), 10573–10588 (2018).